

Improving flight performance of the flapping wing MAV DelFly II

Mark Groen*, Bart Bruggeman*, Bart Remes*, Rick Ruijsink*,
Bas van Oudheusden*, Hester Bijl*

*Faculty of Aerospace Engineering, Delft University of Technology,
Kluyverweg 1, 2629 HT Delft, The Netherlands

E-mail: m.a.groen@student.tudelft.nl b.a.p.bruggeman@student.tudelft.nl
microuav@gmail.com

Abstract. Recent years have seen an increasing interest in micro aerial vehicles (MAVs) and flapping flight in connection to that. The Delft University of Technology has developed a flapping wing MAV, “DelFly II”, which relies on a flapping bi-plane wing configuration for thrust and lift. The ultimate aim of the present research is to improve the flight performance of the DelFly II from both an aerodynamic and constructional perspective. This is pursued by a parametric wing geometry study in combination with a detailed aerodynamic and aeroelastic investigation. In the geometry study an improved wing geometry was found, where stiffeners are placed more outboard for a more rigid in-flight wing shape. The improved wing shows a 10% increase in the thrust-to-power ratio. Investigations into the swirling strength around the DelFly wing in hovering flight show a leading edge vortex (LEV) during the in- and out-stroke. The LEV appears to be less stable than in insect flight, since some shedding of LEV is present.

Nomenclature

<i>Symbol</i>	<i>Description</i>	<i>Unit</i>
f	Wing flapping frequency	Hz
P	Power	W
R	DelFly wing length (semi-span)	mm
T	Thrust	N
λ_{ci}	Positive imaginary part of eigenvalue	-
τ	Dimensionless time	-

Abbreviations

LEV	Leading Edge Vortex
MAV	Micro Aerial Vehicle
UAV	Unmanned Aerial Vehicle

1. Introduction

For the last couple of decades there is an increasing interest in the field of Micro aerial vehicles (MAV's). These MAV's are small unmanned aerial vehicles (UAV's) that find market in both the military and the civil field. These vehicles may employ three different flight concepts: fixed wings, rotary wings or flapping wings. Especially this last type of MAV, the flapping wing type, has very attractive characteristics for flight inside confined spaces. Such an indoor flight capability requires a broad flight envelope. The flyer needs to possess qualities like for example the ability to fly at low speeds, or to hover, high manoeuvrability, low noise emissions and of course it has to be small in size. As demonstrated in previous research^{[1][2]}, flapping flight enables this kind of flight envelope and it has proven to be a potential solution in order to meet the requirements described above.

During the EMAV '05 competition in the summer of 2005, a student design group of Delft University of Technology (DUT) impressed both the jury and the public with the first version of DelFly, the first flapping MAV with vision-based control. DelFly won the price for “Most exotic design”. Since that moment, the interest and research into flapping MAV's has increased at DUT. New research led to an improved version of DelFly, DelFly II. The aim of this development was to

decrease the size while maintaining the flight performance. The wings were optimized based on a trial-and-error approach. DelFly II was smaller in size, more stable and more controllable. In 2008, a third generation of DelFly emerged, DelFly Micro. This version of the flapper with a 100 mm span is even smaller than the previous one, while still carrying a camera on board. Although this flapper is able to fly, it is not yet possible to hover as DelFly II. This is the reason why DelFly II as a proven and well-tested configuration is used as the subject for the current study and not DelFly Micro.

In this study, a detailed research is presented to improve and gain a better understanding of the flight characteristics of DelFly II. In this sense, it presents a continuation of a previous study on DelFly II^[3] in which the flow field around the wings was analyzed by Particle Image Velocimetry (PIV) with simultaneous force measurements performed to indicate the relative contribution of the visualized flow structures to the lift generation. The present study will address the enhanced flow visualization of DelFly by means of phase-locked PIV, as well as the improvement of the DelFly II design. The latter is achieved by improving the aerodynamics and flight characteristics by modifying the wing and changing the stiffeners location and orientation by means of an experimental approach.

1.1. Insect-like flapping flight

As the research is focusing on the hover condition, only the important flow features of this condition will be briefly discussed here. The flow regime under consideration is that of an incompressible, unsteady flow at low Reynolds number. The relatively large forces that are generated during flapping flight cannot be explained with conventional fixed-wing aerodynamic theory. Therefore these forces need to be explained by the presence of the unsteady flow effects and the presence of strong vertical structures in the flow.

Insects use a reciprocating movement of the wings for flight. In figure 1, one can see a schematic approach of one flap cycle. In this movement three phases can be distinguished: the translational phase (moving the wing fore and aft), the rotational phase (when the pitch angle of the wing is changing substantially) and the heaving and plunging phase (upwards and downwards movement of the leading edges). The two half-strokes that make up the flap cycle are called: the down-stroke and the up-stroke. These two strokes are predominantly translational movements. The change in pitch angle during these movements is rather small. At the end of a half-stroke, the rotational phase takes place, during this phase stroke reversal occurs and the wing pitches rapidly.

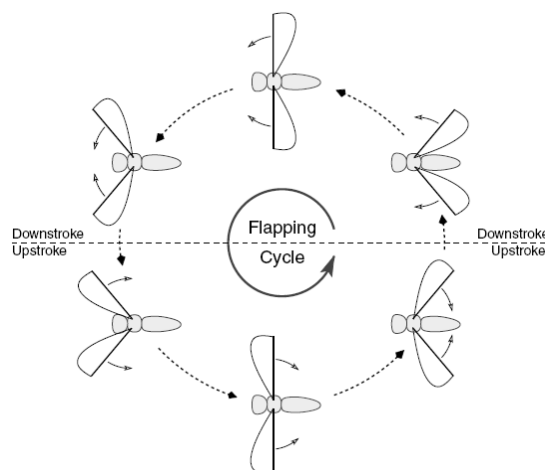


Figure 1. Schematic representation of half strokes during insect flapping. Adapted from Ansari *et al.*^[4].

A detailed description of flapping-flight aerodynamics is outside the scope of the present paper. The mechanics and aerodynamics of insect flapping flight are discussed extensively in reference [5]-[7]. Of the aerodynamic mechanisms that make insect flight possible, the two mechanisms

which are of greatest importance in this study are the occurrence of *leading edge vortices* (LEV's) and the *clap-and-fling* (or in the case of the DelFly the *clap-and-peel*) mechanism. The LEV is the result of flow separation at the wing leading edge, due to the thin airfoil and high angles of attack of the wing. Instead of stalling completely, the wing stall is delayed and the flow is able to reattach further downstream. A LEV is created in the separated part, which adds extra vorticity to the bound circulation of the wing, producing therefore an increase in lift (and also drag, depending on the wing orientation)^[8]. Another mechanism that contributes to the lift production is the clap-and-fling mechanism (or Weis-Fogh mechanism^[9]). It has been discovered that certain insects and birds make use of the clap-and-fling mechanism, sometimes for a limited time in order to generate higher lift during for example the take-off phase^[6]. They do so by increasing the wing stroke to such an extent that the wings touch each other during the dorsal stroke reversal. During the clap the leading edges of the wings touch before the trailing edges do so. When the gap between the wings is closed progressively, the circulation of both wings cancels each other out. The air between the wings is expelled down in the form of a momentum jet enhancing lift^[10], see figure 2 A-C. When the leading edges move away from each other, in the fling phase, air is sucked into the gap that is created. Due to this suction an increase in circulation is generated which means an increase in lift, see figure 2 D-E.

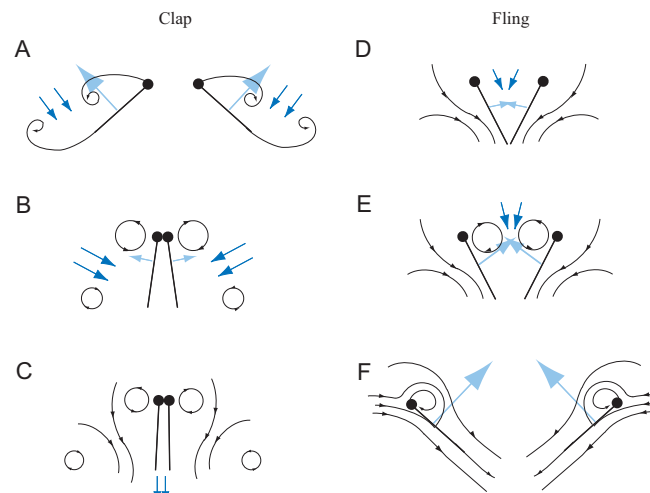


Figure 2. Schematic illustration of the clap-and-fling mechanism; streamlines are illustrated in black, light blue vectors are net forces and dark blue vectors represent the induced velocities. Adapted from Sane^[7].

1.2. DelFly flapping mechanism

DelFly does not use the aerodynamic mechanisms in the same manner as most insects do. The mechanics explained in the previous section are applied to a two-winged insect. DelFly is instead inspired by dragonflies, which have four wings instead of two. The essential difference between the dragonfly's wing configuration and that of DelFly, however, is that DelFly uses a biplane wing configuration with the wings on top of each other while the wings of a dragonfly are behind each other (tandem configuration). Another difference with common insect flight is the heaving and plunging movement that accompanies the flapping. An insect does this actively, whereas this is not the case for DelFly. From high speed camera images however it can be seen that this motion is also present while DelFly is flapping, but it occurs in a passive way. Due to aerodynamic, elastic and inertial forces acting on the wings, the leading edges travel in a "horizontal figure of eight" during one cycle. Finally, the clap-and-peel mechanism that benefits the aerodynamics of DelFly is present in every stroke because of the biplane wing configuration. Clap-and-peel is a variation on the clap-and-fling. Instead of flinging apart more rigidly the wings peel apart due to fluid-structure interaction between the air and the flexible membrane wings. This gives a more gradual build-up of the circulation, which can prevent an unstable LEV from shedding into the wake^[10].

Some characteristics of DelFly are presented in table 1. As all DelFly's are built by hand, no two of them are exactly the same so the weight also differs slightly. With the weight, the wing flapping

frequency required for sustained hovering flight also differs. When a DelFly is hovering, all the energy has to be put in lifting the whole weight of the DelFly. A lower wing flapping frequency is needed in forward flight because of aerodynamic benefits analogous to rotor aircrafts. Under hovering conditions, the Reynolds number based on the mean wing tip velocity and the mean chord is typically of the order of 15,000.

The fuselage frame of DelFly is primarily built out of carbon and balsa wood^[11]. These materials are used because they are light, strong and can be manipulated well. The wings are made from a Mylar foil of 5 μm thickness. This foil is reinforced by carbon stiffeners ($\varnothing 0.28$ mm) which are responsible, together with the aerodynamic forces, for the wing shape during flapping. The leading edges are D-shaped carbon rods (0.7 x 1.4 mm). The DelFly uses a brushless motor for low resistance. Measurements to a brushed motor would prevent accurate measurements due to heating and fast ageing of this type of motor.

Table 1. DelFly Parameters

Parameter	value
Mass	16 – 17 g
Wing flapping frequency	10 – 14 Hz
Flapping angle	48°
Wing length, R	140 mm
Wing span	280 mm
Wing area (one half wing)	1195 mm ²
Aspect ratio	3.5
Mean chord length	80.0 mm
Mean wing tip velocity at 13 Hz	2.73 m/s
Reynolds number ^[12] at 13 Hz	15,000

2. Experimental set-up

An experimental campaign has been conducted to gain a better understanding of the aerodynamic mechanisms during flapping flight and to test various sets of modified wings. In the experimental set-up the upward force generated by the DelFly II was determined as well as the power consumption required for flapping. For a selection of wing configurations additional flow field measurements were carried out using stereoscopic Particle Image Velocimetry (PIV).

In continuation of the research performed by De Clercq^[3], again the choice was made for the hovering flight regime. Since all thrust generated by flapping is needed to stay airborne, hovering flight is the most demanding flight mode within the flight envelope. In comparison to forward flight, unsteady flow features like vortices are expected to be more dominant within the flow in the proximity of the wings. The experimental set-up is designed such that a full-scale DelFly can be fixed to the construction and can be exchanged relatively easy with another model. The set-up has two perpendicularly placed force sensors to measure forces both in the thrust and normal direction, making the set-up also suited for future forward flight measurements.

The first set of experiments focussed on finding an optimized wing geometry. Using a systematic approach new wing geometries were created which are placed on a tailless DelFly II model. The model was mounted on the set-up to measure thrust and power consumption. In this study an optimized wing geometry was found, in terms of maximizing the thrust-to-power ratio. The second experimental campaign focussed on the aerodynamics and aeroelasticity, where PIV was used to study the flow field and the shape of the DelFly II wing.

2.1. Force measurements and DelFly control

For the force measurements and DelFly control, a custom made micro controller board is used. The micro controller board is used to guarantee a high and constant sampling frequency and is connected to a PC with a serial connection. The controller board has a PID-controller which

operates the DelFly motor controller and controls the wing flapping frequency. The wing flapping frequency is measured by counting the motor pulses. Every motor revolution has three motor pulses and given a gear ratio of 1:20 a total of 60 pulses per flap cycle are recorded. The DelFly model is also equipped with a Hall sensor which gives a pulse once every flap cycle to prevent drift. These measurements are used by the controller board to generate a triggering pulse for the PIV system.

Zemic load cells were used to measure the forces. The sensors are of the type Q70x5x9-H with a capacity of 200 g and use strain gauges as sensing element. The sensors are connected to a PICAS amplifier system from Peekel Instruments. This high accuracy measurement system amplifies the measurement signal by approximately a factor of 2000. The PICAS analog output provides the controller board with a -5 V to 5 V signal for a measured range of -0.981 N to 0.981 N. The controller board has a 10 bit A/D-converter which brings the measurement accuracy to 1.92 mN. The same controller board also measures the DelFly supply voltage and current provided by a separate power supply. All measurements are carried out with a sampling frequency of 1860 Hz.

2.2. PIV measurements

Using PIV, the flow around the DelFly II wings is measured by following tracer particles that are illuminated with a laser sheet. The velocity field around the wings is calculated by taking image-pairs of the particles at a small time separation. The experiments are conducted on the original DelFly II wings and on the improved wings from the geometry study. The position of the image plane is varied along the span of the wing, from a position at 60 mm from the wing root to the wing tip at 140 mm. The wing flapping frequency is varied from 9 Hz to 13 Hz, see table 2.

Table 2. Test parameters for the PIV measurements

Wings	Original wing
	Improved wing
Wing flapping frequency	9 Hz
	11 Hz
	13 Hz
Spanwise distance from root	60 mm
	80 mm
	100 mm
	120 mm
	140 mm

The PIV measurements were performed in a phase-locked manner. The pulses from the DelFly motor are used by the controller board to trigger the PIV system every time the DelFly wings are at a certain selected location within the flap cycle. This location can be set in an interface program for the controller board. The PIV measurements are done at intervals of 4% of the flap cycle during the rotational phase of the wing and at intervals of 2% of the flap cycle during the translational phase, producing a total of 34 different locations. For every location 50 phase-locked images are taken, where the final velocity field is an average of these.

To minimize laser light directly reflecting from the wing surface to the cameras, which significantly perturbs the PIV measurement, the laser sheet is oriented perpendicular to the wing surface and the camera viewing directions are placed parallel to the leading edge. The measurements are done on the DelFly upper wing. Results from previous research^[3] showed the velocity field around the bi-plane wing configuration to be symmetrical, which justifies to do the PIV measurements on only one wing. For measurements at different phases in the flap cycle, the DelFly model is rotated around its body to keep the upper wing leading edge perpendicular to the laser sheet. With this set-up the leading edge vortex development is visible without any optical

blockage from the wing itself. Another advantage is the fact that the measurements can be done at a constant spanwise location.

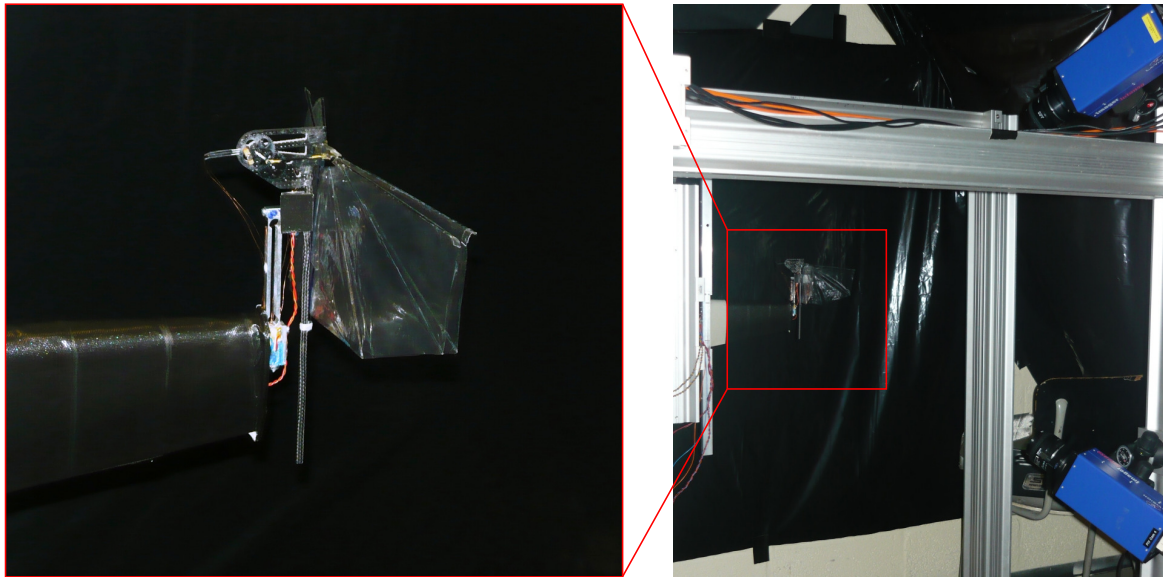


Figure 3. Experimental set-up, with highlighted the tailless DelFly II model

The PIV experiments are conducted on a tailless DelFly II model, see figure 3. The set-up is placed in an enclosed space which is filled with seeding. The seeding is provided by a SAFEX fog generator. The fog generator produces a non-toxic water based fog with droplets with a mean diameter of $1 \mu\text{m}$. A Quantel Twins CFR-400 laser illuminates the model from below. The laser system is a double pulsed Nd:YAG laser. The laser produces infrared light at a wavelength of 1064 nm . A harmonic generator halves the wavelength to 532 nm , which is green light in the visible spectrum. The maximum power is 200 mJ per pulse and the pulse duration is 7 ns . The time delay between pulses is set to $250 \mu\text{s}$.

The flow region of interest is imaged by two LaVision Imager Intense CCD cameras. The LaVision Imager Intense is a high dynamic 12bit cooled CCD camera with a progressive scan sensor. The CCD chip is 1376×1040 pixels with a pixel size of $6.45 \mu\text{m} \times 6.45 \mu\text{m}$, the total size of the CCD chip is $8.9 \text{ mm} \times 6.7 \text{ mm}$. The camera has a double shutter feature, with an interframe time of minimal 500ns to enable PIV measurements. Both cameras are equipped with a lens with a focal length of 35 mm and a daylight filter. The aperture setting for the top camera is different from that of the bottom camera. Since the laser light scatters from the particles primarily in forward direction, the diaphragm of the top camera is more closed to have equal light intensity for both cameras. The final camera and laser settings used for the experiments can be found in table 3.

All image recording and image post processing is done with the software DaVis 7.2 of LaVision. The program triggers the camera and laser when receiving an external pulse from the DelFly controller board and makes it possible to control various settings like laser power and the time between two subsequent images. The post processing function of the program uses correlation to calculate the velocity field from the stereo PIV images. Using images from the two cameras two 2-dimensional velocity fields can be calculated and using stereoscopic PIV all three velocity components in the measurement plane can be determined. Velocity field data is exported to MATLAB for creating velocity plots and further post processing.

Table 3. Settings for the PIV measurements

		camera 1	camera 2
Camera settings	size CCD sensor (pixels)	1376 x 1040	1376 x 1040
	pixel size	6.7 μm	6.7 μm
	field of view	145 x 110 mm^2	145 x 110 mm^2
	magnification, M	0.061	0.061
	optical resolution	105 $\mu\text{m}/\text{pix}$	105 $\mu\text{m}/\text{pix}$
	lens focal length	35 mm	35 mm
	aperture number, $f_{\#}$	11	8
Laser settings	pulse duration	7 ns	
	pulse separation	250 μs	
	wave length	532 nm	
	laser sheet thickness	2.5 \pm 0.5 mm	
Post processing	interrogation window	32 x 32 pixels	
	overlap	50%	
	velocity vector spacing	1.7 mm	

3. Wing geometry

Little previous work has been published about the optimization of the flight performance of such a flapping MAV. Computational approaches for the analysis of a flexible biplane flapping wing configuration are restricted by the difficulties in correctly modelling and simulating the wing-wake interactions. The only way to test the influence of certain parameters is by conducting an experimental study on a real scale Delfly II model. This model was selected in order to reduce the assumptions one has to make if using a non-real model of Delfly II. If only one wing is tested for instance, the influence of clap-and-fling is not taken into account, or if a scaled model is used, Reynolds effects have to be account for, etc.

The different wing parameters are all connected to each other and therefore it is difficult to relate a certain change in performance with a certain single parameter. It can be assumed that the wing area, wing shape, stiffness of the leading edge, stiffness of the stiffeners, Reynolds number, aspect ratio, chord length, wing flapping frequency are all of great influence on the performance in terms of thrust generation and power consumption. To be able to know the influence of a certain parameter, other parameters have to stay fixed. In this research, the influence of the stiffness, orientation and therefore the location of the stiffeners is investigated, while all other parameters are kept constant. Various tests are done with the wing shape and aspect ratio as the changing parameter. Finally the influence of the clap-and-fling on the thrust and power is investigated by looking at a single wing instead of a pair of wings.

3.1. Manufacturing method

In order to have similar results between two nominally identical sets of wings, a well-controlled manufacturing method for constructing and assembling the wings is needed. In many MAV designs, a practical cut-and-glue method is applied, which is simple and cheap. The disadvantage however is that it is not an accurate and repeatable method. Everything is done by hand and therefore there are many uncertainties due to the human factor: the foil tension is different, stiffeners and leading edges are not glued exactly on the same place and this method is time consuming.

Another method is described in reference [13]-[14] and makes use of a Micro-Electro-Mechanical Systems (MEMS) technology. With this technology a titanium substrate is laminated, patterned under UV-light and etched. The result is a “skeleton” of leading edges and stiffeners. The skeleton is now sprayed with parylene-C, the membrane of the wing. This method is very accurate but not suitable for this study at this moment, since the infrastructure for this technology is not yet available and setting up a project like this would lie beyond the scope of this research.

Because of the drawbacks of the previous two methods, another method was developed. This method uses a CNC machine which mills the contours of the wing and location of the stiffeners into a wooden plate. After that, the plate is placed on a vacuum table and Mylar foil is placed on the plate. Because of the vacuum, the Mylar is sucked onto the plate with no extra tension in the foil. The carbon leading edges and stiffeners can now be glued to the Mylar with great precision into the grooves. When everything is glued, the CNC machine cuts the wing contour. This method is much faster than the normal cut-and-glue method and the wing is manufactured with much more control.

3.2. Influence of stiffener position

The focus of this test lies on the influence of stiffener orientation. The orientation of the stiffeners was systematically approached, while the shape and area of the wing was not changed. First, the two stiffeners were positioned parallel to each other under five different angles with the trailing edge (TE): 0°, 31°, 63°, 77°, 90°. The location and wing shape can be seen in figure 4. Each wing is tested for 20 seconds at different frequencies. The quoted experimental values of thrust and power are the average values over that time interval. The results of these tests can be seen in figure 5. Wing31 and wing63 (respectively with the stiffeners under an angle of 31° and 63° with the TE) give the best thrust-to-power ratio. The higher the thrust-to-power ratio (T/P), the more thrust generation for a lower power consumption. The wing without stiffeners (Wing Clean) has poor characteristics. For frequencies higher than 11.5Hz, the system failed. The same is true for wing77. The reason for failure at 11.5Hz is not yet known.

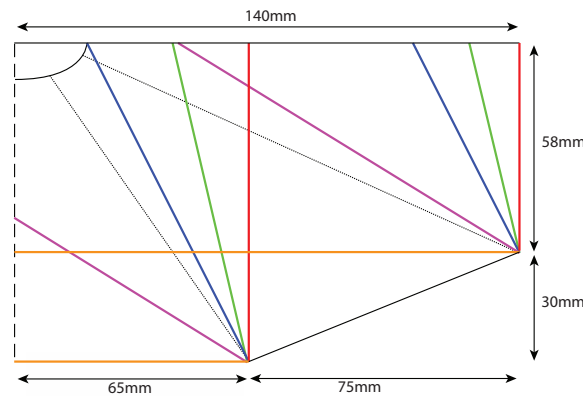


Figure 4. Schematic representation of half wing with stiffener location of wing0 (orange), wing31 (purple), wing63 (blue), wing77 (green), wing90 (red) and wing standard (dotted)

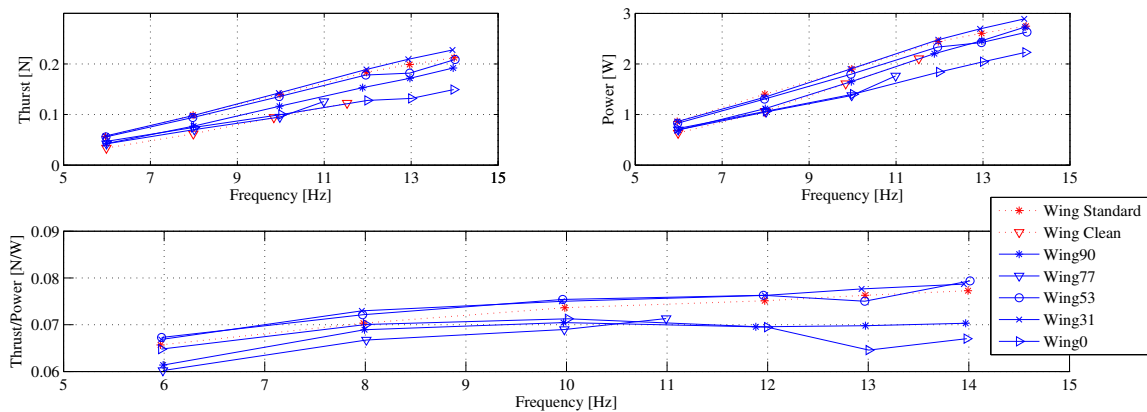


Figure 5. Performance plots of wings with parallel stiffeners

This set of wings was also tested with a rigid connection between the leading edges and the stiffeners in order to increase the overall stiffness of the wings. When the average values of thrust and power versus flapping frequency were plotted, a small increase in thrust could be observed for every set of wings, but also an increase in power. The two resulted in a decrease in thrust-to-power ratio for every wing with a rigid connection. No further tests are done with such rigid connections.

To improve the performance of the wing even more, combinations of wing31 and wing63 are built, which result in wing6331 (blue) and wing3151 (purple), see figure 6. The first two numbers represent the angle of the inner stiffener with the TE and the last two numbers represent the angle of the outer stiffener. The inner angle of wing3151 is increased otherwise the stiffener could penetrate through the foil, this happened with wing31. Plots of the performance showed that wing6331 was the better of the two. For this wing, the stiffeners converge from the trailing edge to the leading edge of the wing. In figure 7, different types of converging stiffener configuration (with upper and lower limit of the angles set by wing6331) are illustrated. Six different configurations are tested and the performance can be seen in figure 8.

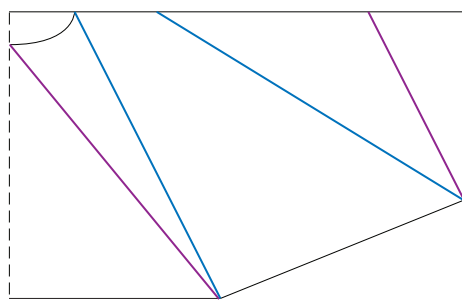


Figure 6. Wing6332 and wing3151

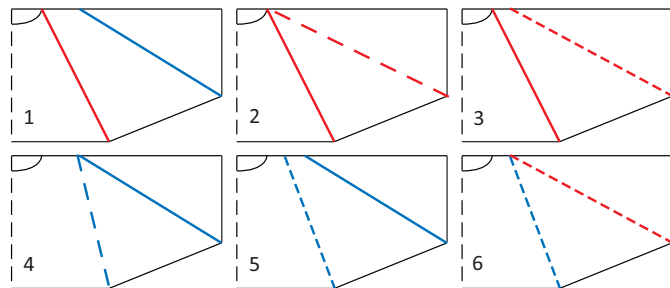


Figure 7. Converging stiffener configurations

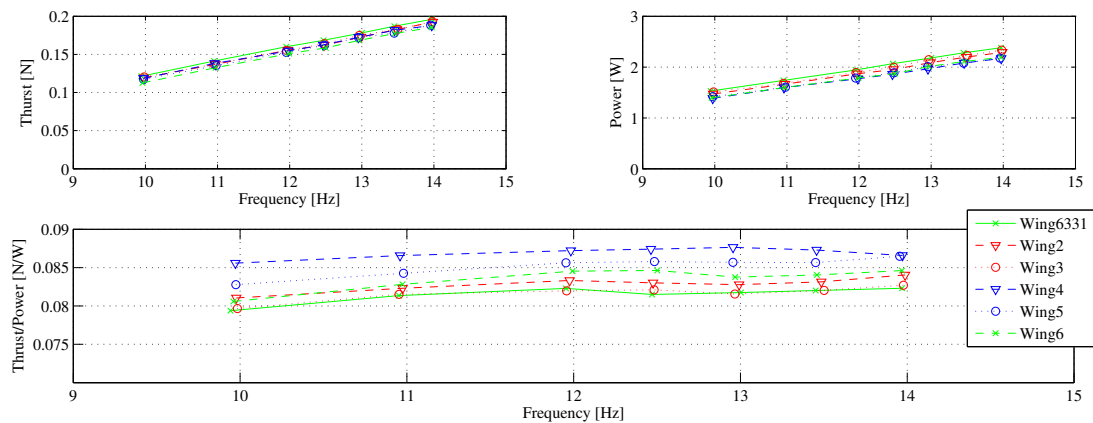


Figure 8. Performance plots of converging stiffeners combinations

Wing configuration 4, from figure 7, has the best thrust-to-power ratio of all configurations. The stiffeners are converged and meet each other at the leading edge. The thrust generation for the fully converged wing is not as high as for wing6331, but the increase in power consumption for wing6331 results in a lower thrust-to-power ratio. The improved wing with new stiffener configuration has an increase in thrust-to-power ratio of 10% with respect to the original DelFly II wing configuration. This wing is used in the aerodynamic study described in section 4.

3.3. Influence of stiffener diameter

The influence of stiffener diameter (and therefore also the influence of its stiffness) is investigated by changing it from the standard 0.28 mm up to a maximum of 1.0 mm, see table 4. The difference in inner and outer diameter of the stiffener will result in a different deformation during flapping. This can be translated to a difference in thrust generation and power consumption. From figure 9 it

can be observed that the thrust and power increase with the increase of cross-section area of the stiffener. The thrust-to-power ratio, however, decreases with increasing cross-sectional area. A wing with 0.28 mm stiffeners has the best characteristics. The wing with 1.0 mm diameter stiffeners is not plotted in figure 9 because the mechanism failed at wing flapping frequencies of 10Hz and higher. This wing is relatively heavy in comparison to the other wings and therefore the motor controller was unable to control the wing flapping frequency due to high inertial forces.

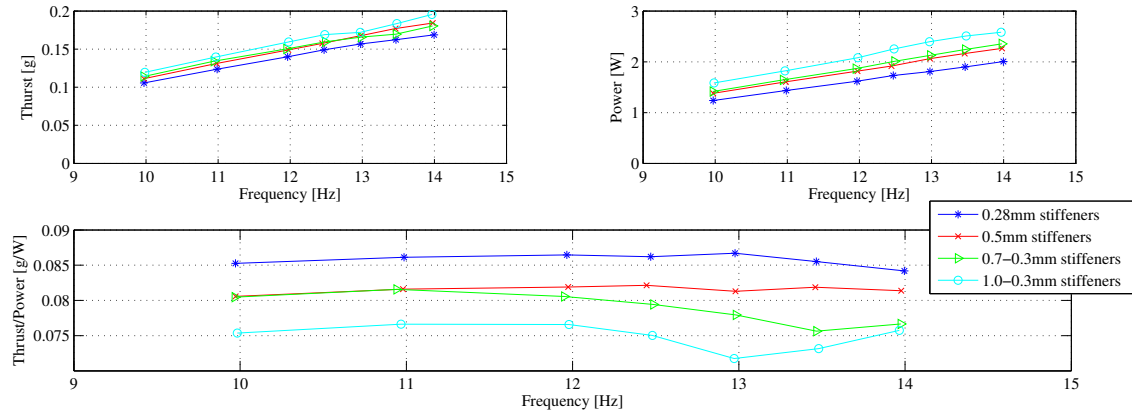


Figure 9. Performance plots of wings with different stiffener thickness

Table 4. Stiffener properties

Diameter [mm]	Wing mass [g]
0.28	1.1
0.5	1.3
0.7 (outer) - 0.3 (inner)	1.4
1.0 (outer) - 0.3 (inner)	1.7
1.0	2.2

3.4. Clap-and-peel effect for DelFly

DelFly makes use of the clap-and-peel mechanism to gain extra thrust (lift) force. To investigate the exact gain in thrust, a single DelFly wing was tested on the model to assess the performance of one single wing. The difference between the thrust generation of the biplane configuration and twice the thrust generation of a single wing is interpreted as the interaction, i.e. the “clap-and-peel effect”. Figure 10 shows a plot of thrust versus frequency for a single wing (blue diamonds) and a biplane configuration (red stars). The thick solid line (blue) represents the doubled values of the single wing. From this figure it can be seen that an additional 6% in thrust is gained due to the clap-and-peel effect of DelFly II. This is much lower than the gain that insects get from this aerodynamic mechanism, which is generally assessed to be around 25% on average. A study on a 10 cm MAV of 2.3 g^[16] showed an increase in thrust due to clap-and-fling which is strongly related to relative wind speed. The higher the relative wind speed, the greater the clap-and-fling benefit. This can explain the difference, because the tests in this study are done for hover condition.

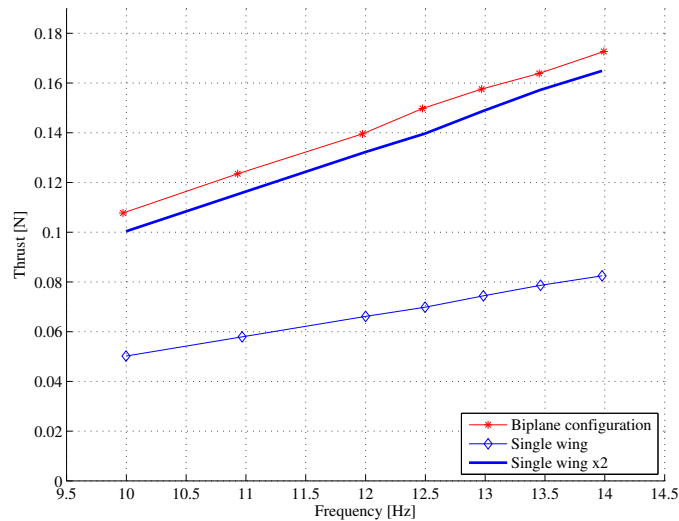


Figure 10. Effect of clap-and-peel on DelFly

4. Aerodynamics and aeroelasticity

In order to obtain further insight into improvement in flight mechanics, a detailed experimental study is performed of the aerodynamics and aeroelasticity of the DelFly II. Here the flow dynamics as well as the wing deformation is studied by means of Particle Image Velocimetry (PIV). At the same time thrust and power consumption are recorded, so these can be related to the instantaneous flow field structures in any phase within the flap cycle.

4.1. DelFly wing deformation

The wings used on DelFly II are made from Mylar foil with carbon stiffeners and a D-shaped carbon rod for the leading edge. The in-flight wing shape is determined by aerodynamic, elastic and inertial forces. The aerodynamic forces are in turn influenced by the wing shape, leading to a complex fluid-structure interaction. Determination of the in-flight wing shape is important to help explain aerodynamic effects. They can also be used as an input for numerical flow simulations of flapping flight, such as the work of F.M. Bos *et al.*^[17] or as a benchmark for future full fluid-structure interactions simulations.

To compare the original DelFly II wing with the improved wing, the wing shape is extracted from images taken during the PIV experiments. In figure 11 the wing shape of the original DelFly II wing at various moments during the flap cycle is shown for the non-dimensional time, $\tau = t/T$, where T is the flapping period. In figure 12 this is shown for the improved wing. For both figures the cross-sections are taken at 100 mm from the root ($0.71R$) and the wing flapping frequency is 11 Hz. From figure 11 it can be seen that the original DelFly II wing is more flexible during the rotation ($\tau = 0.5$) than the improved wing. The stiffeners on the new wing are placed more outboard compared to the stiffeners on the original wing. This gives the improved wings more rigidity at locations near the wing tips.

The wing shape of both wings during the translation (both in-stroke as out-stroke) are comparable. The path of the leading edge of both wings describes a figure of eight. The cross-sections in figure 11 and figure 12 show the foil folded over the D-shaped leading edge carbon rod. The orientation of the carbon rod gives rigidity in the stroke direction but allows the leading edge to bend up and down more easily. Previous research has shown this to have a positive effect on the thrust generation.

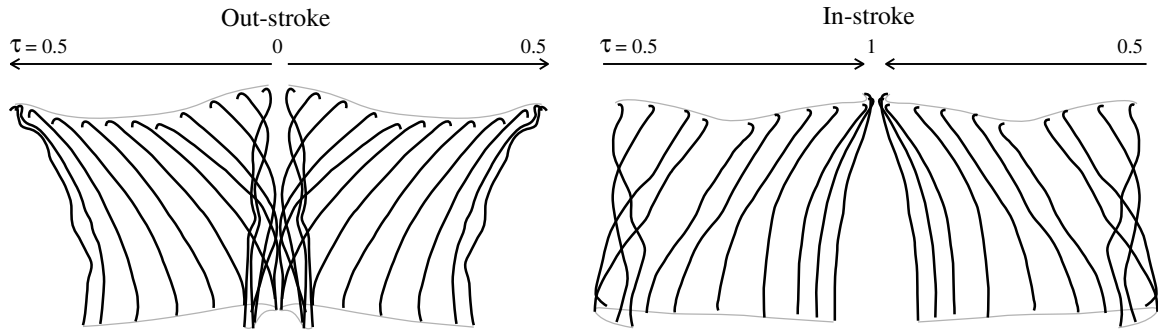


Figure 11. Cross-sections of the original wing during a flap cycle at a wing flapping frequency 11 Hz at a spanwise location of 100 mm from the root ($0.71R$).

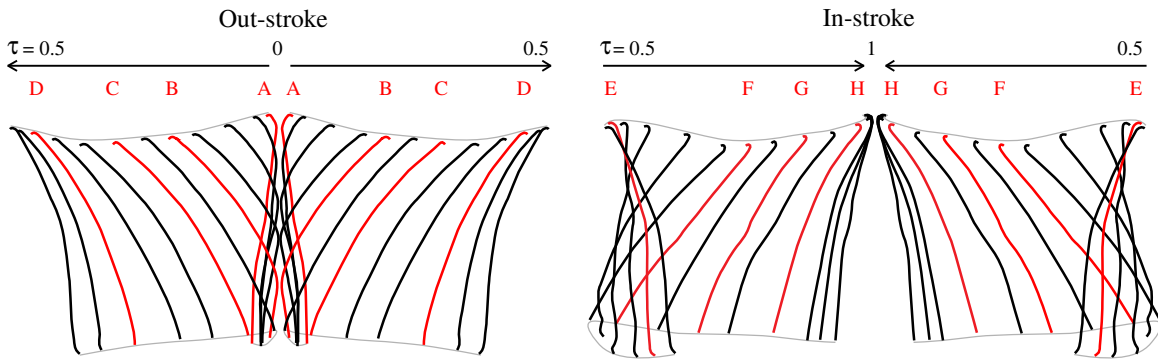


Figure 12. Cross-sections of the improved wing during a flap cycle at a wing flapping frequency 11 Hz at a spanwise location of 100 mm from the root ($0.71R$).

4.2. DelFly force and power measurements

In the geometry study, described in section 3, thrust and power consumption are measured for various wings. The averaged thrust over a number of flapping cycles is plotted against wing flapping frequency. Figure 10 shows a clear linear increase in thrust with frequency. To relate the thrust and power consumption during a flap cycle to the flow field, they have been measured during the PIV measurements. Unfortunately the thrust measurements suffered from severe mechanical resonance in the force measurement system. The high accuracy force sensors act as a relatively soft spring. Together with the DelFly model the natural frequency of the whole system lies within the measurement range. Extra tests in a vacuum chamber have shown only the first two modes of vibration (twice the forcing frequency) can be ascribed with certainty to aerodynamic forces. To eliminate the vibrations caused by resonance of the set-up, a low pass filter has been constructed to examine the thrust generation within a flap cycle. The passive low pass filter, based on a Fourier transformation, has a cut-off frequency of twice the forcing frequency. A disadvantage of using this filter is that all aerodynamically related thrust fluctuations with a small characteristic time are also filtered out.

Figure 13 shows the thrust during one flap cycle for various frequencies scaled for the non-dimensional time, τ . The thrust generated during the out-stroke is higher than during the in-stroke. Previous research^[3] has contributed this to the fact that at the beginning of the out-stroke the peel mechanism contributes to extra thrust. A comparison between the original wing and the improved wing shows little difference in the thrust generation. The geometry study already showed the average thrust to vary little. The improvement of the new wing is mainly found in the power consumption. A comparison of the power consumption shows the improved wing to have an overall smaller power consumption over the whole flap cycle. This could mean an overall

improvement in drag, which is not measured for each wing individually. Since the improved wing also shows reduced power consumption in vacuum, the improvement is also elastic-mechanical.

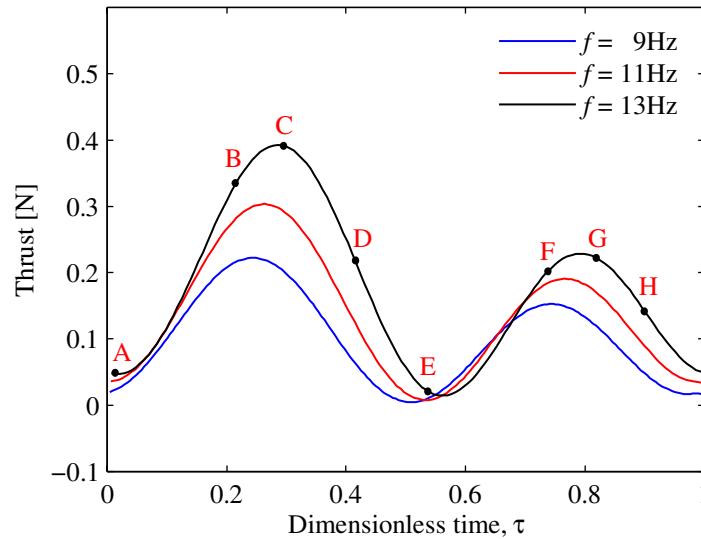


Figure 13. Thrust generated during a complete flap cycle

4.3. DelFly flow field measurements

The flow field around the DelFly wings is studied using stereoscopic PIV, which provides all three velocity components in the plane of the laser sheet. The in-plane velocity components are used to investigate the vortex dynamics in the cross-sectional plane normal to the wing leading edge. The out-of-plane velocity component represents the velocity component parallel to the leading edge.

For the investigation of the vortex development, the velocity field is used to calculate swirling strength instead of vorticity, since vorticity does not only identify vortex cores but also shearing motion within the flow. The location of vortex cores is determined from the swirling strength, which is calculated according to the method of R.J. Adrian *et al.*^[18]. The swirling strength of a local swirling motion is quantified by λ_{ci} , the positive imaginary part of the eigenvalue of the local velocity gradient tensor.

In figure 14 the swirling strength at various moments during the flap cycle is shown for the improved wing at a spanwise location of 100 mm from the root ($0.71R$). A wing flapping frequency of 13 Hz is used, since at this frequency enough thrust is generated to sustain hovering flight. The corresponding phase in the flap cycle is shown in figure 12. In figure 14 it is shown that at both the in-stroke and out-stroke at the trailing edge a strong starting vortex is generated that is sustained during the next half-stroke. Halfway during the out-stroke a leading edge vortex (LEV) is generated (B), which is (partially) shed (C) and grown back to larger strength (D). At the beginning of the in-stroke (E) the LEV is dissipated. Halfway during the in-stroke another LEV is generated (F), which again appears to be (partially) shed (G) and grown back (H). At the beginning of the out-stroke (A) when the leading edges touch, the vortices interact and dissipate when the leading edges start moving apart again. It can be seen that during the translation a LEV is present. The LEV does not appear to be as stable as in insect flight^{[8][19]}, as some vortex shedding is observed. This could be due to the relative high Reynolds number. DelFly operates at a Reynolds number of 15,000 while insects fly at Reynolds numbers varying from 10 to 10,000.

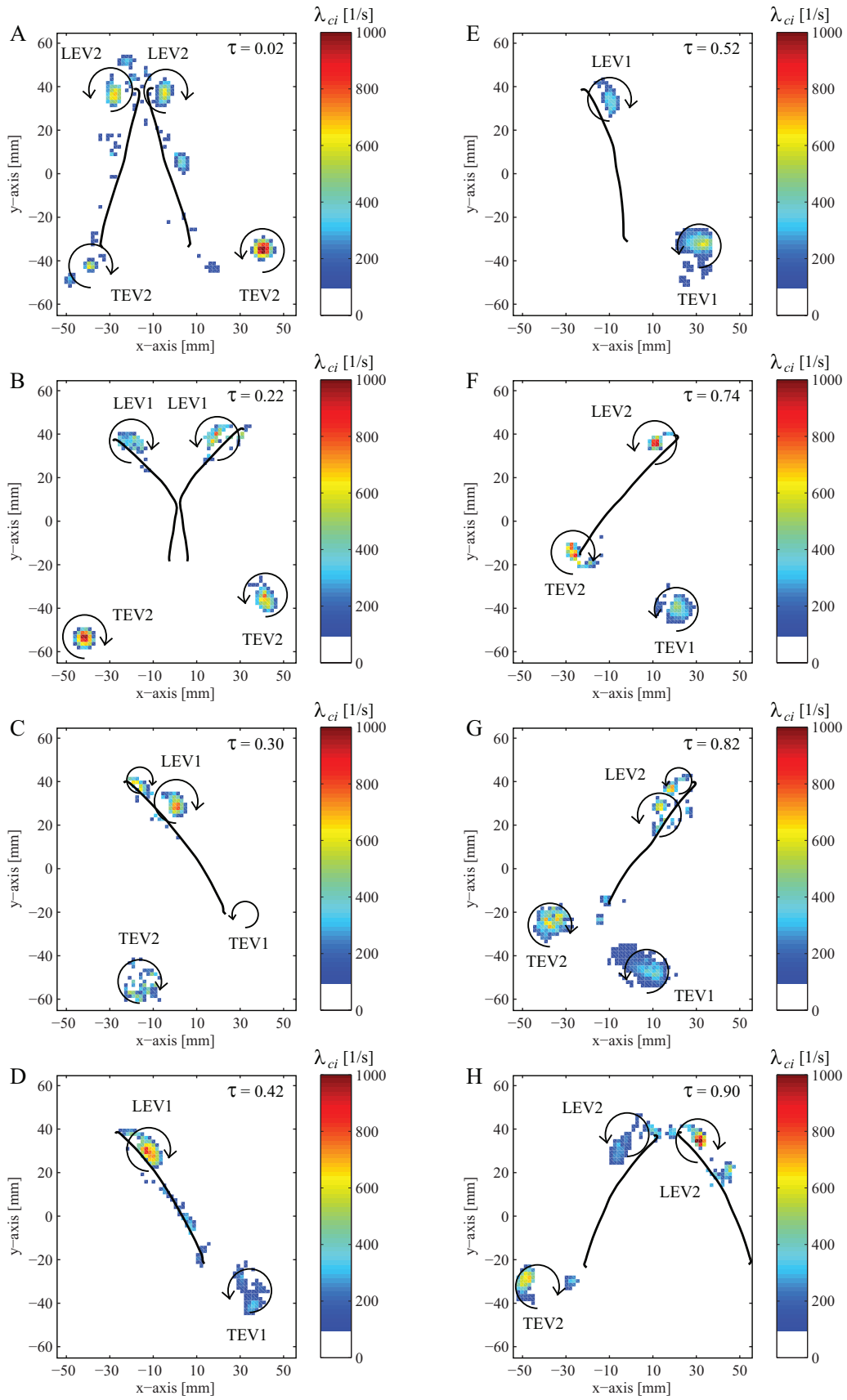


Figure 14. Swirling strength at various moments during the flap cycle, showing leading edge vortices (LEV) and trailing edge vortices (TEV) during out-stroke (1) and during in-stroke (2). The swirling direction is taken from velocity field images.

Examination of the spanwise variation of the vortex development shows a conical growth from spanwise locations near the root to the tip. At the wing tip, however, all vortices are no longer present in the investigated flow region. Also the LEV shedding is shown along the span. In figure 15 the swirling strength during the in-stroke at $\tau = 0.84$ is shown for three spanwise locations. Between $0.57R$ and $0.86R$ the LEV grows and a partial shedding is shown at $0.71R$ and at $0.86R$. At the wing tip no swirling is present in the plane normal to the leading edge. Investigations into the out-of-plane velocity in insect flight^[19], show a axial flow present within the LEV for high Reynolds numbers. The current research also shows the presence of axial flow in the vortex core where the out of plane velocity component is as large as the wing tip velocity at a spanwise position of $0.86R$.

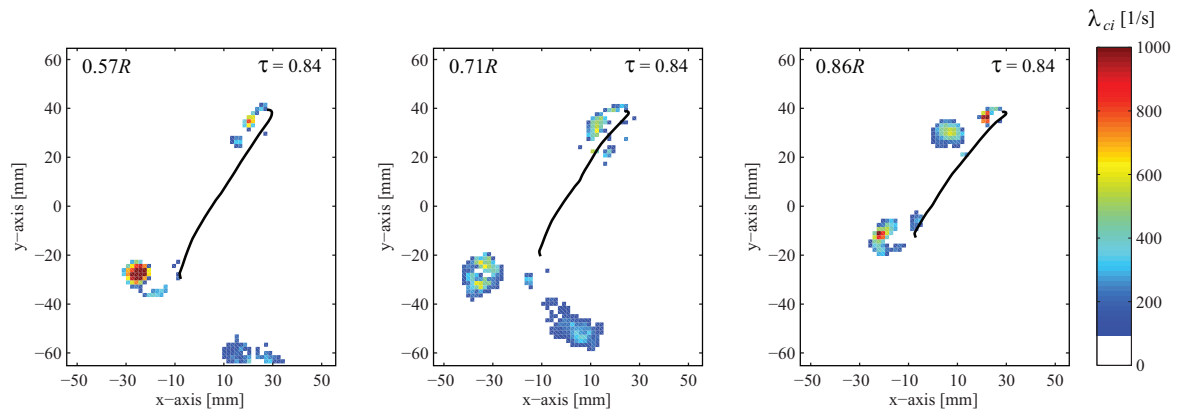


Figure 15. Swirling strength at various spanwise positions for $\tau = 0.84$

One parameter to change the Reynolds number is changing the wing flapping frequency. In figure 16 the swirling strength is shown for wing flapping frequencies varying from 9 Hz to 13 Hz at a spanwise location of $0.71R$ at $\tau = 0.78$. The LEV is present at all frequencies as is the partial shedding halfway during the in-stroke. Not just for this figure but for the whole flap cycle it can be said, that for a wing flapping frequency of 13 Hz, vorticity is concentrated more closely to the wing surface. Further investigations into changing Reynolds number and spanwise vortex development are currently being conducted by studying high aspect ratio wings.

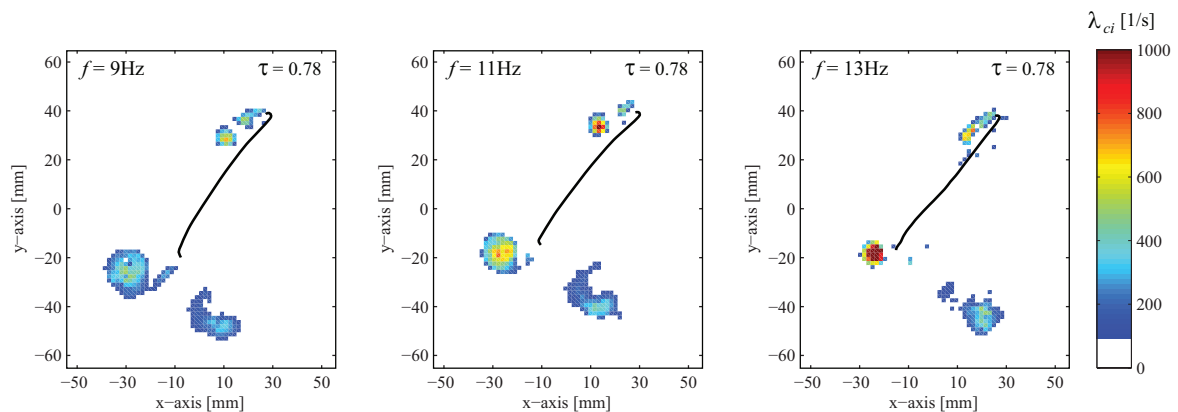


Figure 16. Swirling strength at various flapping frequencies for $\tau = 0.78$

5. Conclusions and recommendations

An experimental campaign was conducted to improve the flight performance of the flapping wing MAV DelFly II. Also an aerodynamic and aeroelastic study has been performed using PIV.

The cut-and-glue method for building DelFly wings was found inefficient and inaccurate for this study. A new method was found by augmenting the traditional cut-and-glue method with vacuum

technique and usage of a CNC-machine. This method is faster, more accurate and the wings perform better than the traditional built wings.

Changing the DelFly wing-geometry affects the flight characteristics and performance of DelFly. Increasing stiffener thickness was found ineffective. Although thrust increases, the thrust-to-power ratio reduces. By optimizing stiffener orientation, an increase of 10% in the thrust-to-power ratio of the system is obtained. From the PIV images it can be seen the improved wing shows a more rigid rotation, than the original wing. The largest increase in performance is found in the power consumption. The increase in thrust is smaller, because the driving parameters for the thrust (wing area, Reynolds number, stroke angle) are kept constant. The power consumption is reduced over the complete flap cycle, which could mean an improvement in drag. Since the improved wing also shows reduced power consumption in vacuum, the improved wing is also an elastic-mechanical improvement.

The influence of clap-and-peel is investigated for DelFly. Clap-and-peel results in an increase in thrust. When the wings clap together a momentum jet enhancing lift is created and when the wings peel apart air is sucked in between enhancing circulation. The thrust generated during the out-stroke is therefore higher than for the in-stroke. For DelFly, clap-and-peel results in a 6% increase in thrust.

Investigations into the swirling strength around the DelFly wing in hovering flight show a leading edge vortex (LEV) during the in- and out-stroke. The LEV appears to be less stable than in insect flight, since some shedding of LEV is present. The vortices are larger at the outboard span locations, but no longer present at the tip.

Investigations of the out-of-plane velocity show a spanwise velocity within the vortex core. More investigations into the 3-dimensional vortex structure around the DelFly wing and the effect of Reynolds number is being conducted. Future research will focus on forward flight of a complete DelFly model. It is known the tail has important effects on performance and stability. Further investigations are proposed for tail effects.

References

- [1] Żbikowski, R. "Flapping Wing Autonomous Micro Air Vehicles: Research Programme Outline", *14th International Conference on Unmanned Air Vehicle Systems, Bristol Univ., Bristol, England, U.K.*, pp. 38.1–38.5 (1999)
- [2] Ansari, S.A.; Żbikowski, R.; Knowles, K. "Aerodynamic Modelling of Insectlike Flapping Flight for Micro Air Vehicles", *Progress in Aerospace Sciences*, Vol. 42 (2), pp. 129 – 172 (2006)
- [3] De Clercq, K.M.E.; De Kat, R.; Remes, B.; Van Oudheusden, B.W.; Bijl, H. "Flow visualization and force measurements on a hovering flapping-wing MAV DelFly II", *39th AIAA Fluid Dynamics Conference, San Antonio, Texas, AIAA 2009-4035* (2009)
- [4] Ansari, S.A.; Knowles, K.; Żbikowski, R. "Insectlike Flapping Wings in the Hover Part 2: Effect of Wing Geometry", *Journal of Aircraft*, Vol. 45 (6), pp. 1976 – 1990 (2008)
- [5] Ellington, C.P. "Unsteady Aerodynamics of Insect Flight", *Symposia of the Society for Experimental Biology*, Vol. 49, pp. 109 – 129 (1995)
- [6] Lehmann, F.O. "The Mechanisms of Lift Enhancement in Insect Flight", *Naturwissenschaften*, Vol. 91 (3), pp. 101 – 122, (2004)
- [7] Sane, S.P. "The Aerodynamics of Insect Flight", *Journal of Experimental Biology*, Vol. 206 (23), pp. 4191 – 4208 (2003)
- [8] Ellington, C.P.; Van den Berg, C.; Willmott, A. P.; Thomas, A. L. R., "Leading-Edge Vortices in Insect Flight", *Nature*, Vol. 384, pp. 626–630 (1996)
- [9] Weis-Fogh, T. "Quick estimates of flight fitness in hovering animals, including novel mechanisms for lift production", *Journal of Experimental Biology*, Vol. 59, pp. 169 – 230 (1972)
- [10] De Clercq, K.M.E. "Flow visualization and force measurements on a hovering flapping-wing MAV DelFly II", Delft University of Technology M.Sc. thesis (2009)
- [11] De Croon, G.C.H.E.; De Clercq, K.M.E.; Ruijsink, R.; Remes, B.; De Wagter C. "Design, aerodynamics, and vision-based control of the DelFly", *International Journal of MAV*, Vol. 1 (2), pp 71 – 97 (2009)

- [12] Ellington, C.P. "The Novel Aerodynamics of Insect Flight: Applications to Micro-Air Vehicles", *Journal of Experimental Biology*, Vol. 202, pp. 3439 – 3448 (1999)
- [13] Pornsin-Sirirak, T.N.; Tai, Y.C.; Nassef, H.; Ho, C.M. "Unsteady-state Aerodynamic Performance of MEMS", *International Symposium on Smart Structures and Micro Systems*, Vol. 1, pp G1-2 (2000)
- [14] Pornsin-Sirirak, T.N.; Tai, Y.C.; Nassef, H.; Ho, C.M. "Titanium-alloy MEMS Wing Technology for A Micro Aerial Vehicle Application", *Sensors and Actuators, A: Physical*, Vol. 89 (1-2), pp 95-103 (2001)
- [15] Marden, J.H. "Maximum lift production during takeoff in flying animal", *Journal of Experimental Biology*, Vol. 130, pp. 235 – 258 (1987)
- [16] Kawamura, Y.; Souda, S.; Nishimoto, S.; Ellington C.P. "Clapping-wing Micro Air Vehicle of Insect Size", *Biomedical and Life Sciences*, Part 3, pp. 319 – 330 (2008)
- [17] Bos, F.M.; Lentink, D.; Van Oudheusden, B.W.; Bijl, H. "Influence of wing kinematics on aerodynamic performance in hovering insect flight", *Journal of fluid mechanics*, Vol. 594, pp. 341 - 368 (2008)
- [18] Adrian, R.J.; Christensen, K.T.; Liu, Z.C. "Analysis and interpretation of instantaneous turbulent velocity fields", *Experiments in Fluids*, Vol. 29, pp. 275-290 (2000)
- [19] Birch, J.M.; Dickson, W.B.; Dickinson, M.H. "Force production and flow structure of the leading edge vortex on flapping wings at high and low Reynolds numbers", *Journal of Experimental Biology*, Vol. 207 (7), pp. 1063 – 1072 (2004)